Experiments with Rayleigh-Bénard convection

Guenter Ahlers

Department of Physics and IQUEST, University of California
Santa Barbara CA 93106 USA
e-mail: guenter@physics.ucsb.edu

Summary. After a brief review in the Introduction of the major breakthroughs in the study of Rayleigh-Bénard convection (RBC) since the experiments of Henri Bénard, a few selected topics are presented in more detail. The effect of thermal noise on the bifurcation to convection is discussed because experimental work on this is quite recent and as yet incomplete. Examples of spatio-temporal chaos are examined because this interesting nonlinear state is as yet incompletely understood. The effect of rotation on RBC is presented because some of the experimental results disagree with modern theories.

1 Introduction

Convection in a shallow horizontal layer of a fluid heated from below had been observed on several occasions during the 19^{th} Century.[1] However, the carefully controlled and quantitative laboratory experiments of Henri Bénard [2] focused the interests of other scientists on this fascinating problem. Bénard studied the patterns of the convective flow in the presence of a free upper surface, using a variety of fluids with different viscosities. He made quantitative determinations of the deformation of the upper surface, of the characteristic length scales of the pattern, and of the direction of flow within the fluid. Although we now know that the beautiful hexagonal patterns observed by Bénard [3] were caused by the contribution of a temperature dependent surface tension, these experiments were the direct motivation of Lord Rayleigh's seminal stability analysis [4] for the case of free horizontal boundaries in the *absence* of surface tension. Rayleigh's opening remark in his paper in *The London, Edinburgh, and Dublin Philosophical Magazine and Journal of Science* was "The present is an attempt to examine how far the interesting results obained by Bénard in his careful and skilful experiments can be explained theoretically". Lord Rayleigh recognized that there is a finite value of the temperature difference $\Delta T = \Delta T_c$ for the onset of convection, and that the important combination of parameters which determines the onset is

$$R = \frac{\alpha g d^3 \Delta T}{\kappa \nu} \tag{1}$$

where α is the isobaric thermal expansion coefficient, κ the thermal diffusivity, ν the kinematic viscosity, d the spacing between the plates, g the acceleration of gravity, and ΔT the temperature difference. We now refer to R as the "Rayleigh

number". Lord Rayleigh also found that the instability occurs at finite wavenumber k_c, and that it is a stationary instability (*i.e.* that the relevant eigenvalues are real). For the free boundary conditions that he used he was able to obtain the analytic results $R_c = 27\pi^4/4$ and $k_c = \pi/\sqrt{2}$.

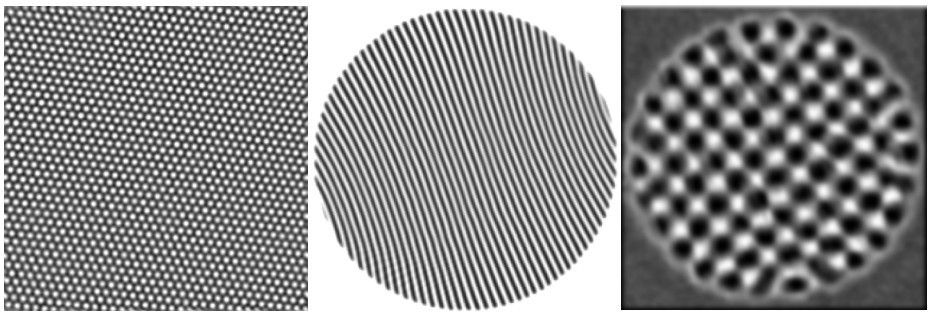

Fig. 1. Left: hexagonal pattern of non-Boussinesq convection in compressed SF_6 near its critical point (from [6]). Middle: roll pattern for a Boussinesq fluid (from [7]). Right: Square pattern in binary-mixture convection (from [8]).

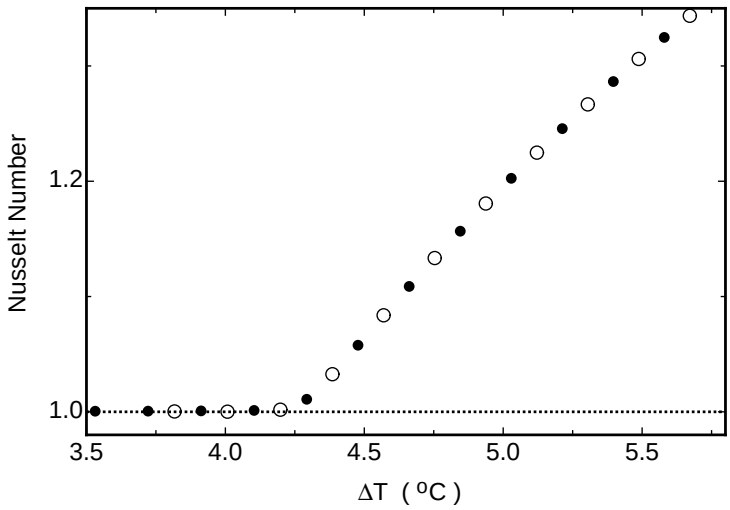

Fig. 2. Nusselt number measurements using ethanol in a circular cell with $d = 1.54$ mm and diameter $D = 88$ mm. Open (closed) circles: increasing (decreasing) ΔT (from [14]).

The problem caught the attention of other giants in the field during the next several decades. Here I mention only a few highlights. Rayleigh's work was followed by the stability analysis for more realistic *rigid* boundaries by Sir

Harold Jeffreys, [5] which (after some numerical problems) yielded the values $R_c = 1708$ and $k_c = 3.117$ relevant to experiments using fluids confined between well-conducting solid parallel plates. There was a number of other milestones. Particularly noteworthy on the theoretical side were the first weakly non-linear analyses which led to predictions of the stable convection patterns. On the basis of the linear stability analysis of Lord Rayleigh or Sir Harald Jeffreys one knows the magnitude of the critical wave director, but one can not decide whether the patterns above onset will consist of rolls, hexagons, or squares. Indeed all three patterns occur in RBC as illustrated in Fig. 1, [6, 7, 8] albeit under different circumstances. Malkus and Veronis [9] predicted that the stable planform for the case of free boundaries and Boussinesq conditions [10, 11] should be straight rolls rather than *e.g.* squares or hexagons. The foundation for much of the "modern" work on Rayleigh-Bénard convection was laid during the 1960's by the weakly nonlinear analysis of Schlüter, Lortz, and Busse (SLB) [12] for *rigid* boundaries, which predicted stable straight rolls above onset also for this realistic case. This prediction is in agreement with experiment, as illustrated by the middle pattern of Fig. 1 as well as by numerous other experiments. SLB also established that the bifurcation to RBC is supercritical, and gave the initial slope S_1 of the Nusselt number $\mathcal{N} \equiv Qd/\lambda\Delta T = 1 + S_1\epsilon + \mathcal{O}(\epsilon^2)$ (λ is the conductivity of the quiescent fluid and Q is the heat current density). This was consistent with early measurements, for instance with those of Silveston [13]. Modern measurements like those shown in Fig. 2, [14] even within their much greater resolution, are also consistent with a supercritical bifurcation. However, the experimental value of S_1 varies somewhat from one experiment to another and is always somewhat lower than the theoretical prediction (for the data in Fig. 2 $S_1 = 1.28$ whereas the prediction is $S_1 = 1.43$). Possibly this problem is due to boundary effects at the sidewall, but this issue is not entirely settled. Conceptually the next great step forward was the realization by Swift and Hohenberg [15] that the bifurcation to RBC, shown by SLB to be supercritical in the deterministic system, becomes subcritical in the presence of thermal noise. Although at the time the first-order nature of the transition was believed to become significant only within a part per million or so of the transition, thus being out of reach of the experimentalist, good evidence for it has been obtained in very recent experiments [16].

Equally important were seminal experimental contributions during the first five or six decades following Bénard's work. Here I mention only a couple. The heat transport measurements of Schmidt and Milverton [17] confirmed the prediction $R_c = 1708$ with an accuracy of better than 10 %. The extensive experiments of Silveston [13] already mentioned above provided data for $\mathcal{N}$ from below onset to $R \simeq 5 \times 10^6$. Silveston also visualized the convection patterns in his apparatus, using the shadowgraph method which has become so very important in more recent times [18, 19, 20]. For additional historical notes, the reader may wish to consult the article by P. Mannevill in this volume, and the informative book by Chandrasekhar [1].

During the last three decades Rayleigh-Bénard convection (RBC) has become a paradigm for the study of pattern formation [21]. It reveals numerous

interesting phenomena in various ranges of $\epsilon \equiv \Delta T/\Delta T_c - 1$. Many of these phenomena have been studied in detail recently, using primarily compressed gases as the fluid, sensitive shadowgraph flow-visualization, digital image analysis, and quantitative heat-flux measurements [19, 22]. I briefly mention some of them here, and then discuss a few of these in greater detail in separate sections below.

Even below onset, thermally driven fluctuations of the temperature and velocity fields about their pure conduction averages provide a fascinating example of critical phenomena in a non-equilibrium system. Already 27 years ago it was predicted by Swift and Hohenberg [15] that these fluctuations should alter the nature of the bifurcation to RBC, making it subcritical and thus analogous to a first-order phase transition in equilibrium systems. Very recent measurements [16] suggest that this is indeed the case.

Above but close to onset the pattern for a Boussinesq system consists of straight rolls (see Fig. 1 middle), possibly with some defects induced by the sidewalls [23]. When non-Boussinesq conditions prevail, a pattern of perfect, defect-free hexagons evolves (see Fig. 1 left).

Further above onset, for $\epsilon > 0.5$ or so, an interesting qualitatively different state of spatio-temporal chaos, known as spiral-defect chaos (SDC), occurs in systems with Prandtl numbers $\sigma \equiv \nu/\kappa$ of order one or less. [24] This state is a bulk property and not sidewall induced; it has been studied intensely by theorists as well as experimentalists.

Similarly, RBC was used to study the onset of time dependence over a wide range of σ. [25, 26] Temporally periodic or chaotic patterns were found for $\epsilon > \mathcal{O}(1)$, with the onset occurring at smaller ϵ for smaller σ. However, quantitative studies like those carried out for SDC are still lacking at larger σ.

The system becomes more complex and interesting even near onset when it is rotated about a vertical axis with an angular velocity $\mathbf{\Omega}$. For that case it was predicted [27, 28, 29] and found experimentally [30, 31, 32] that, for $\Omega > \Omega_c$, the primary bifurcation from the conduction state remains supercritical and leads to parallel rolls which are *unstable*. The instability is to plane-wave perturbations with a wave-director angle which is advanced relative to that of the rolls by an angular increment Θ_{KL} in the direction of $\mathbf{\Omega}$. This phenomenon is known as the Küppers-Lortz (KL) instability. The pattern consists of domains of rolls which incessantly replace each other, both by irregular domain-wall motion and by the KL mechanism. The spatial and temporal behavior suggests the term "domain chaos" for this state. Since this example of spatio-temporal chaos occurs directly at onset, it should be more accessible to theoretical elucidation than, for example, the spiral-defect chaos mentioned above.

Theoretically, the KL instability is expected to persist near onset up to large values of Ω. Thus it was a surprise that the patterns found in experiments near onset changed dramatically when Ω was increased.[33] For $\Omega \geq 70$, there was no evidence of the characteristic domain chaos until ϵ was increased well above 0.1. At smaller ϵ, four-fold coordinated cellular patterns, and in some parameter ranges slowly-rotating, aesthetically appealing, square lattices, were encountered.

Relatively unexplored are experimental opportunities which RBC has to offer in the range of σ well below unity. Pure fluids (with rare exceptions [34]) have $\sigma \geq 0.7$. Recently it was shown [35, 36] that smaller values of σ can be reached by mixing two gases, one with a large and the other with a small atomic or molecular weight. The most extreme example readily available is a mixture of H_2 and Xe. Prandtl numbers as small as 0.16 can be reached. In the range $\sigma \leq 0.6$, several interesting new phenomena are predicted to occur. [29, 37, 38] In the $\sigma - \Omega$ plane they include subcritical bifurcations below a line of tricritical bifurcations, Hopf bifurcations to standing waves, a line of codimension-two points where the Hopf bifurcation meets the stationary bifurcation, and a codimension-three point where the codimension-two line and the tricritical line meet.

Another rich and interesting modification of the Rayleigh-Bénard system is achieved by inclining the layer relative to gravity. [39, 40, 22] This adds the tilt angle γ as an additional parameter. In this case the basic state consists of heat conduction and a parallel shear flow which breaks the rotational invariance of the usual RBC. Depending on γ and σ, longitudinal, oblique, transverse, and travelling transverse rolls are the possible flow structures at onset.

No doubt I neglected to mention additional important topics associated with RBC. Nonetheless, at this point we will proceed to a somewhat more detailed review of a few of the phenomana listed above which I have found particularly interesting.

2 Fluctuations near the Onset of Convection

In the usual deterministic description of RBC, based on the Boussinesq or Navier-Stokes equations, all velocities vanish below the onset of convection and the temperature is given by the pure conduction profile. However, the Brownian motion of the atoms or molecules which occurs because the system is at a finite temperature leads to fluctuations of the temperature and velocity fields which have zero mean but finite mean square. When the fluctuation amplitudes are small enough, their interactions with each other can be neglected and the amplitudes can be described well by stochastic linearized hydrodynamic equations. [41] To my knowledge, the first spatially extended non-equilibrium system for which quantitative measurements of these fluctuations were made was electroconvection in a nematic liquid crystal [42]. Soon thereafter, thermally driven fluctuations were observed also for RBC, [43] and quantitative measurements of their amplitudes were made. [44, 45] In part these measurements were made possible by the development of experimental techniques for the study of RBC in compressed gases.[23, 19] There it is possible to use sample spacings an order of magnitude smaller than for conventional liquids and kinematic viscosities are relatively small, thus making the systems more susceptible to noise. In addition, maximizing the sensitivity of the shadowgraph method and careful digital image analysis have enhanced the experimental resolution.[19]

In the left part of Fig. 3 we show a processed image of a layer of CO_2 of thickness 0.47 mm at a pressure of 29 bars and at a mean temperature of 32.0°C.

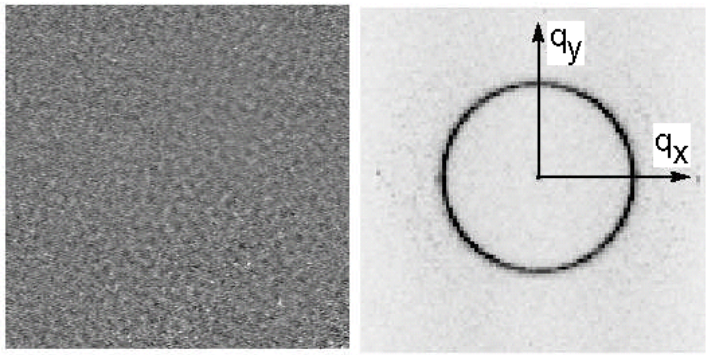

Fig. 3. Left: Shadowgraph snapshot of fluctuations below the onset of convection ($\epsilon = -3 \times 10^{-4}$). Right: The average of the square of the modulus of the Fourier transform of 64 images like that on the left. After [44].

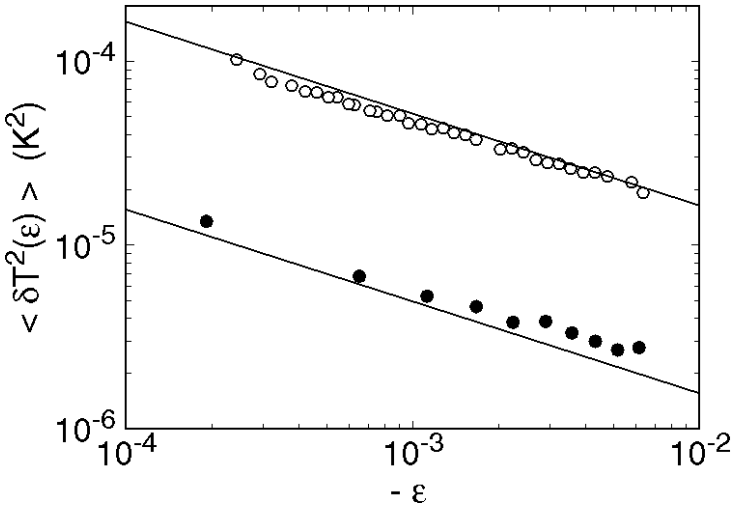

Fig. 4. Mean square amplitudes of the temperature fluctuations below the onset of convection of a layer of CO_2 of thickness 0.47 mm and a mean temperature of $32^\circ C$. The solid (open) circles are for a sample pressure of 42.3 (29.0) bars. The two lines are the theoretical predictions. Note that there are no adjustable parameters. After [44].

The sample was at $\epsilon = -3 \times 10^{-4}$, very close to but just below the bifurcation point. The fluctuating pattern is barely detectable by eye. The right half of the figure shows the average of the structure factors (squares of the moduli of the Fourier transforms) of 64 such images. It demonstrates clearly that the fluctuations have a characteristic wavenumber q. The value of q is in quantative agreement with the critical wavenumber $q_c = 3.117$ for RBC. The ring in Fourier space is azimuthally uniform, reflecting the continuous rotational symmetry of the RBC system.

The power contained within the ring in Fourier space can be converted quantitatively to the mean-square amplitude of the temperature field.[44, 19, 22] Results for the temporal and spatial averages $\langle \delta T^2 \rangle$ of the square of the deviations of the temperature from the local time average (pure conduction) as a function of ϵ at two different sample pressures are shown in Fig. 4 using logarithmic scales. The data can be described quite accurately by straight lines with slopes close to -1/2, consistent with the powerlaw $\langle \delta T^2 \rangle \propto \epsilon^{-1/2}$ as predicted by linerar theory.

The amplitudes of the fluctuating modes below but close to the onset of RBC were calculated quantitatively from the linearized stochastic hydrodynamic equations[41] by van Beijeren and Cohen[46], using realistic (no-slip) boundary conditions at the top and bottom of the cell. For the mean square temperature fluctuations their results give[47, 44]

$$\langle \delta T^2(\epsilon) \rangle = \tilde{c}^2 \left(\frac{\Delta T_c}{R_c} \right)^2 \frac{F}{4\sqrt{-\epsilon}} \quad , \tag{2}$$

with $\tilde{c} = 3q_c\sqrt{R_c} = 385.28$. Here $R_c = 1708$ is the critical Rayleigh number, and the noise intensity F is given by

$$F = \frac{k_B T}{\rho d \nu^2} \times \frac{2\sigma q_c}{\xi_o \tau_o R_c} \quad , \tag{3}$$

with $\xi_o = 0.385$ and $\tau_o \simeq 0.0796$. One sees that F depends on the density ρ and kinematic viscosity ν, as well as on the Prandtl number $\sigma = \nu/D_T$ (D_T is the thermal diffusivity). Using the fluid properties of the experimental samples,[19] one obtains the straight lines in Fig. 4. Since there are no adjustable parameters, the agreement between theory and experiment can be regarded as excellent. This agreement lends strong support to the validity of Landau's stochastic hydrodynamic equations[41].

Sufficiently close to the bifurcation, where fluctuation amplitudes become large, nonlinear interactions between them play a role and linear theory breaks down. In this regime genuine critical phenomena which differ from the linear predictions are expected, and the precise critical behavior should depend on the symmetry properties and the dimensionality of the system. Deviations from the prediction of linear theory have been observed recently for electroconvection in nematic liquid crystals [48, 49] which is exceptionally susceptible to the influence of thermal noise. Unfortunately to this day there are no predictions of the critical phenomena to be expected for this interesting group of systems. For RBC,

Swift and Hohenberg were able to show that the system belongs to the same universality class as one considered by Brazovskii.[15, 47, 50] Equilibrium systems belonging to this class include the crystallization of di-block co-polymers.[51] For this universality class the transition is of second order at the mean-field level, but the fluctuations induce a first-order tarnsition. A common feature of all the systems belonging to this class is that the order parameter near the bifurcation has a relatively large volume of phase space accessible to it. In the RBC case this is reflected in the rotational invariance of the system as demonstrated by the *ring* in Fourier space shown in Fig. 3. On the basis of this qualitative consideration one would not expect the electroconvection system mentioned above[48, 49] to belong to the Brazovskii universality class because the anisotropy due to the director leads to only one or two pairs of spots in Fourier space.

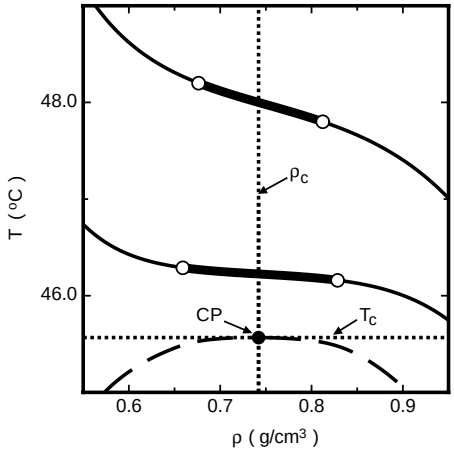

Fig. 5. The temperature-density plane near the critical point of SF_6. The dashed line is the coexistence curve separating liquid and vapor. The vertical dotted line is the critical isochore. The solid circle is the critical point $T_c = 45.567°$C, $P_c = 37.545$ bars and $\rho_c = 0.742$ g/cm^3. The solid lines represent the isobars $P = 38.10$ bars (lower line) and 39.58 bars (upper line) used extensively in experiments. The heavy solid lines, each ending in two circles, illustrate the density range spanned during measurements with $\Delta T \simeq \Delta T_c$ for a cell of spacing $d = 34.3\mu$m (lower line) and $d = 59.1\mu$m (upper line).

For RBC in ordinary liquids one can estimate[15] that nonlinear fluctuation effects should be observable typically only for $|\epsilon| \leq 10^{-6}$, which has not been accessible to experiments so far. For RBC in compressed gases the critical region is a bit wider, reaching as far out as $|\epsilon| \simeq 10^{-5}$; but as can be seen from Fig. 4, this too has been beyond experimental resolution. However, the situation is much more favorable near a liquid-gas critical point (CP). [16] Part of the reason for this can be seen by inspecting Eq. 3. and the phase diagram of SF_6 shown in Fig. 5. In that figure we see the temperature-density plane near the CP. The vertical dotted line corresponds to the critical isochore, and the two solid

lines are isobars. As the CP is approached on the critical isochore from higher temperatures, the viscosity ν has only a mild singularity and remains finite, whereas the Prandtl number $\sigma = \nu/D_T$ diverges because the thermal diffusivity D_T vanishes. Thus the divergence of σ at finite ν leads to a divergence of F.[52] An equally important aspect is, however, that the fluid properties are such that typical sample spacings d which can be used are in the range of 10 to 100 μm, thus increasing F by one or two orders of magnitude compared to liquids and compressed gases away from the critical point. Another factor which greatly increases the experimental shadowgraph resolution near the CP is the value of the temperature derivative of the refractive index dn/dT. Typically we have $|dn/dT| \simeq 0.1$, whereas for ordinary fluids it tends to be two or three orders of magnitude smaller.

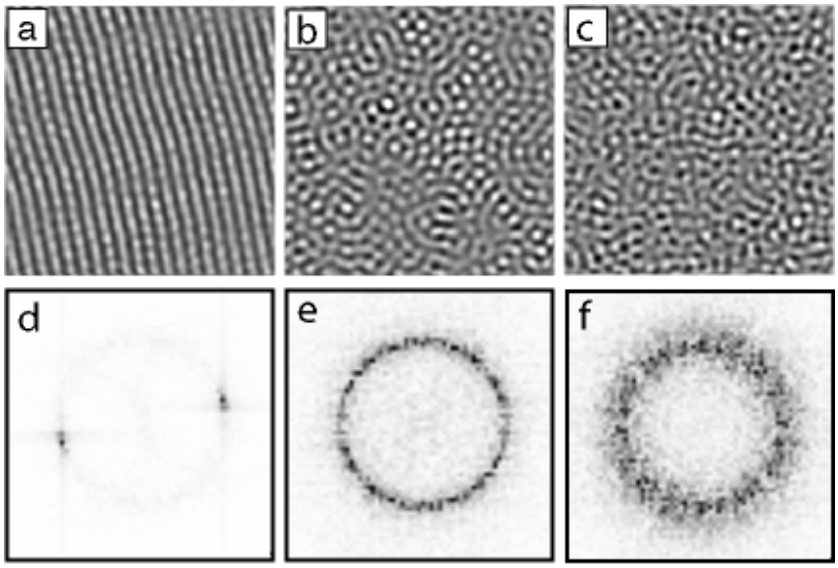

Fig. 6. Shadowgraph images (top row) of a 1.28×1.28 mm^2 part of a sample with $d = 34.3$ μm, and the moduli of their Fourier transforms (bottom row). From left to right, the images are for $\epsilon = 0.008$, -0.001, and -0.047. The mean temperature and the pressure corresponded to the critical isochore at $T = 46.22°$C. Adapted from Ref. [16]

In Fig. 6 we show shadowgraph snapshots of fluctuations and roll patterns for a cell of spacing $d = 34.3$ μm at a pressure $P = 38.10$ bars corresponding to the lower isobar shown in Fig. 5. [16] The mean temperature $\bar{T} = 46.22°$C was kept constant during the experiment and had a value which corresponded to the critical isochore. When the applied temperature difference was equal to $\Delta T_c = 0.131°$C, the sample occupied the heavy section of the line representing the isobar. The theoretical value of F was 5×10^{-4} for this case. The images are for several ϵ values. The bottom row shows the moduli of their Fourier transforms. Just above onset the pattern consisted of convection rolls, as predicted for the

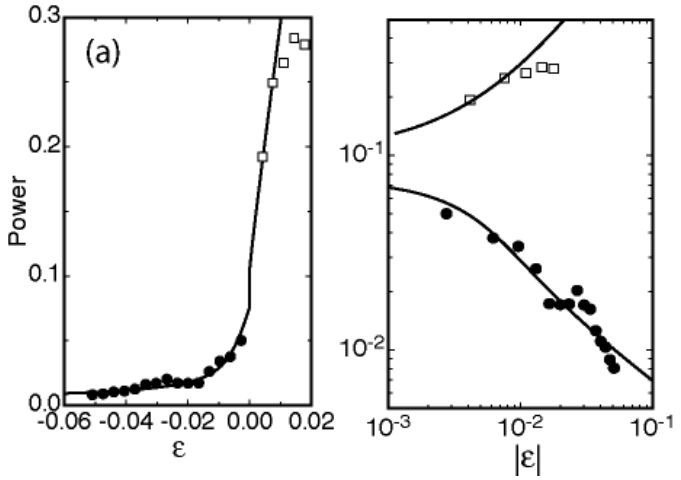

Fig. 7. Shadowgraph power $\mathcal{P}$ as a function of $\epsilon \equiv \Delta T/\Delta T_c - 1$ for the experiment of Fig. 6 on a) linear and b) logarithmic scales. Solid lines: fit of the Swift-Hohenberg prediction [47] to the data. From Ref. [16]

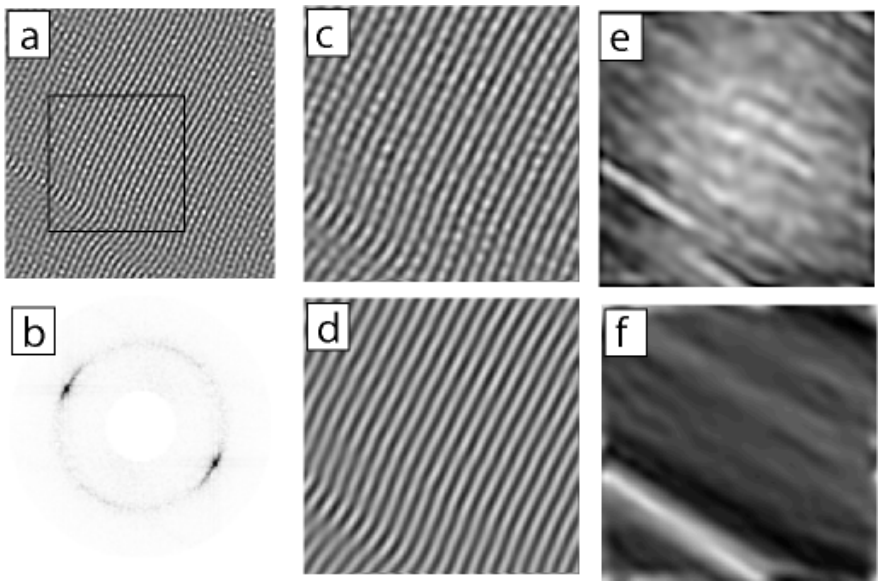

Fig. 8. Patterns from a sample with $d = 59$ μm at $\epsilon = 0.009$. (a): image of size 1.92×1.92 mm^2 and b) the modulus of its Fourier transform. (c): the 0.96×0.96 mm^2 area inside the square in (a). (d): same area as (c), but after a bandpass filter was applied around the Fourier-transform peaks of (b). (e): amplitude of the rolls of (a) obtained by Fourier-transform demodulation. (f): director angle of (a). Adapted from Ref. [16]

deterministic system.[12] Consistent with the Swift-Hohenberg prediction of a first-order transition, there was a sharp transition from a pattern of rolls to one of disordered fluctuating cellular structures as ΔT was decreased below ΔT_c.

Figure 7 gives results for the shadowgraph power (the square of the modulus of the Fourier transform) as a function of ϵ. One sees a dramatic change in the power at $\epsilon = 0$. The solid lines are a fit of the prediction of Swift and Hohenberg to the data. This fit yielded $F = 7 \times 10^{-4}$, in good agreement with the prediction based on the fluid properties.

Aside from the order of the transition, an issue of considerable interest is the nature of the ordered state (*i.e.* the rolls) above onset. In Fig. 8 we show an example. [16] One sees that the rolls reveal several types of disorder. Particularly in the enlarged image Fig. 8c it can be seen that the rolls were modulated along their axis. This was the result of the superposition of fluctuations of random orientation. As seen in Fig. 8d, it could be removed by band-pass Fourier filtering with the filters centered on the two peaks of the transform shown in Fig. 8b. A second type of disorder took the form of an amplitude modulation which varied irregularly in time and space. A snapshot of the roll amplitude, obtained by Fourier demodulation, is shown in Fig. 8e. A third type of disorder took the form of roll undulations; *i.e.* a variation of the angle of the roll director along the roll axis. A grey-scale rendering of the director angle, obtained from a local wavedirector analysis [55], is shown in Fig. 8f. We see that both the roll amplitude and the director-angle modulation are correlated over relatively long distances in the direction of the wave director, and vary much more rapidly along the roll axis. Some of this noise-induced disorder had been anticipated by Toner and Nelson, [56] and should have a commonality with disorder near phase transitions in other two-dimensional systems.

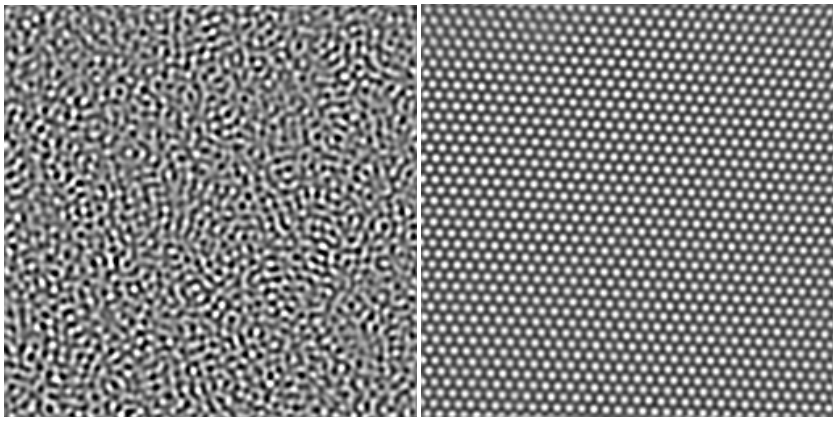

Fig. 9. Shadowgraph images of a 1.92×1.92 mm^2 part of a sample with $d = 59$ μm and a pressure of 39.58 bars. Left: $\epsilon = -0.0015$. Right: $\epsilon = 0.0025$. The mean temperature was 48.3°C.

Interestingly, rolls are encountered above the bifurcation only when the mean sample temperature is such that the density corresponds to the critical density. Figure 9 shows the fluctuations just below (left image) and the ordered pattern just above (right image) the bifurcation for an experiment in which the mean temperature was 48.3°C. [6] At the pressure of the experiment (39.58 bars) the critical density would have been achieved at 48.0°C. One sees that a dislocation-free lattice of hexagons forms. Although the hexagons are reminiscent of Henri Bénard's beautiful patterns, they have their origin in non-Boussinesq effects [57, 58] whereas Bénard's hexagons were caused by a temperature dependent surface tension. Measurements of the hysteresis associated with the formation and disappearance of the hexagons in Fig. 9, as well as a transition to rolls at larger ϵ, were in quite good agreement with predictions based on the deterministic equations of motion [57] even though fluctuations were present. [59]

3 Deterministic patterns

When the effective noise intensity is relatively small, the system above onset can be understood in terms of the deterministic equations of motion. The formation of deterministic patterns takes many forms and depends on such parameters as the Prandtl number, the aspect ratio, and the shape of the sidewalls. Any attempt at a thorough review is well beyond the scope of this article. As an example of the richness of pattern-formation phenomena which are encountered I show in Fig. 10 some shadowgraph images for $\sigma = 1.0$ and $\Gamma = 28.7$ in a cylindrical cell. [60] For this case $F = 1 \times 10^{-7}$, and stochastic effects do not play an important role. The patterns were obtained with compressed CO_2 as the fluid, but the values of σ and Γ are fairly close to those studied by Croquette and coworkers [23] using Argon under pressure and to those of Hu *et al.* [61] using CO_2. Some of Croquette's results are shown in the chaper by Manneville in this volume. Croquette found that a time independent pattern existed only close to onset, roughly for $\epsilon < 0.12$. As ϵ increased, the rolls developed an increasing tendency to terminate with their axes orthogonal to the sidewall. The consequent roll curvature and the associated mean flow caused a compression of the rolls near the cell center. For ϵ close to 0.12 the wavenumber in the interior crossed the skewed-varicose instability-boundary [62] and a temporal succession of dislocation pairs was formed, thus rendering the pattern time dependent. Most likely this process provides the explanation of the time dependence observed close to onset by heat-transport measurements in early cryogenic convection experiments. [63, 64]

As ϵ increased, the patterns became more complex as illustrated in Fig. 10 for $\epsilon = 0.45$. Typically three wall foci existed at this point. Because of the associated roll curvature there were mean-flow fields emanating from the foci. These flows were strong enough to cause a continuous emission of traveling convection rolls from the foci, leading to a complicated dynamics in the cell interior.[61] These patterns were, however, sidewall induced and not intrinsic to the interior of a very large system. This was shown in an experiment where the walls were replaced

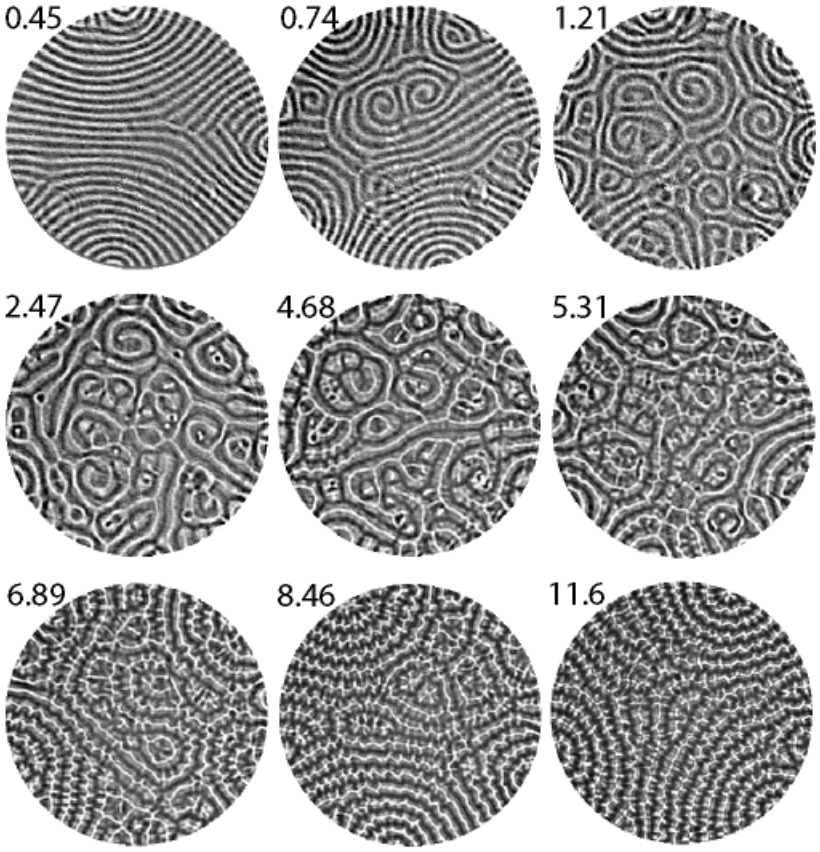

Fig. 10. Shadowgraph images for CO_2 at a pressure of 33.25 bars and mean temperature of 21.16°C in a cell with $d = 1.5$ mm and aspect ratio $\Gamma = 28.7$. The Prandtl number was 1.0 and ΔT_c was found to be 0.317°C. The number near each image gives the value of $\epsilon = \Delta T/\Delta T_c - 1$. After Ref. [60]

by a very gentle radial ramp in the cell spacing which led to a region of pure conduction surrounding the convecting interior. [7] An example of a pattern in this system, for $\epsilon = 0.21$, is shown in the middle of Fig. 1. In that case one found time independent near-perfect rolls without defects and with relatively little roll curvature.

Somewhere near $\epsilon = 0.8$ a new phenomenon occurred. Small spirals formed in the interior, as illustrated in Fig. 10 for $\epsilon = 0.74$ and 1.21. The formation of these spirals was an intrinsic property of the bulk convection system and was not induced by the sidewalls. This state, known as spiral-defect chaos, has been known to exist only for the last decade or so [24] and is discussed in more detail in Sect. 4.2 below.

As ϵ increased further, the structures became more disordered and the spirals were a less dominant feature as seen at $\epsilon = 2.47$. The next interesting

phenomenon was first noticeable for $\epsilon = 4.68$, and became more pronounced as ϵ increased to the larger values. This was a transverse perturbation of the convection rolls by a moduation which had a relatively short wavelength. This new feature was due to the oscillatory instability predicted by Clever and Busse. [65] These transverse modulations of the rolls were traveling waves which moved along the roll axes.

The evolution with increasing ϵ seen for the last three patterns is remarkable. Although the patterns became more complex in the sense that the oscillatory modulation became more pronounced, on a coarse-grained scale which averages over the traveling waves they became simpler again. Thus, the pattern at $\epsilon = 11.6$ was not unlike the one for $\epsilon = 0.45$; both had three wall foci and similar defect structures in the interior. It would be nice to be able to understand this reduction of complexity with increasing stress.

4 Spatio-temporal chaos

4.1 Early Measurements

The early 1970's brought a broad survey over a wide range of Prandtl numbers of the occurrence of time dependent patterns in RBC [25, 26]. At about that time quantitative studies of the statictical properties of spatio-temporal chaos (STC) for σ near one were carried out on RBC at cryogenic temperatures. [66, 67, 68, 69] This early work was followed soon by quantitative measurements [70, 71] on *temporal* chaos in systems without significant spatial extent which, for some time, attracted far more attention because they made contact with concurrent theoretical developments [72]; this interaction between theory and experiment revived the field of dynamical systems as a branch of physics. [73] By now this field has reached a certain level of maturity. Here I want to examine some of the experimental results on chaos in systems with significant *spatial* variation. For these the level of theoretical understanding is still much more limited than it is for dynamical systems. [74]

Results for the time-averaged Nusselt number $\langle \mathcal{N} \rangle$ during the early cryogenic experiments (for which there was no flow visualization) are shown in Fig. 11a as a function of $\epsilon \equiv \Delta T/\Delta T_c - 1$. A surprise at the time of those measurements was that the convection depended non-periodically on the time t already at the relatively small values $\epsilon \simeq 1$. This is illustrated in Fig. 11b for a circular cell with an aspect ratio Γ (radius/height) = 5.3 and $\epsilon = 1.23$. The power spectrum of $\mathcal{N}(t)$ was broad, with a maximum at the frequency $f = 0$, and for large f it fell off as f^{-4} as shown in Fig. 11c. The experimentally observed algebraic falloff was surprising because simple models of chaos in deterministic systems with relatively few degrees of freedom, such as the Lorenz model, have a spectrum with an exponential falloff. [75, 76] It seems likely [67] that the onset of time dependence was associated with an adjustment of the wavenumber k as a function of ϵ which caused the system to cross an instability boundary, from our present vantage point most likely the skewed-varicose (SV) instability. [62]

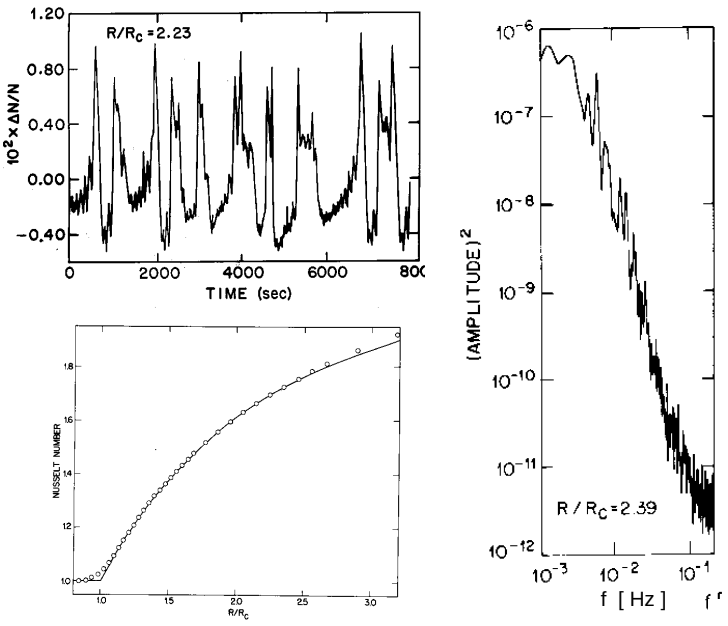

Fig. 11. Results from RBC at cryogenic temperatures. (a): the time-averaged Nusselt number as a function of ϵ. (b): typical deviations of the Nusselt number from its mean for $\epsilon = 1.23$ as a function of time. (c): the power spectrum of a longer sequence of data like those in (b) for $\epsilon = 1.23$. After Ref. [68].

The apparently algebraic falloff of the spectrum presumably is then attributable to the presence of a large number of chaotic interacting modes in the spatially extended system which turns out to lead to effectively algebraic decay [75, 76] over the experimentally accessible range of f; but so far as I know a quantitative explanation of this phenomenon is still lacking. In a qualitative sense this suggestion that many modes come into play as the spatial extent increases is an early indicator that spatio-temporal chaos is high-dimensional, and perhaps *extensive* in the sense that the number of modes (or basis functions) needed to describe it is proportional to (or at least increases with) the system size. [77]

In order to provide a quantitative characterization of the chaotic state, the square root of the variance $\sigma_{\mathcal{N}}$ of $\mathcal{N}(t)$ as well as the first moment f_1 of its power spectrum were determined as a funtion of R. As R increased, it turned out that the chaotic state was entered with a discontinuous jump of $\sigma_{\mathcal{N}}$ from zero, and that f_1 was finite at onset. With increasing R, f_1 followed a powerlaw over the two decades $1 < \epsilon < 200$, with an exponent close to 2/3. To this day I am not aware of a theoretical explanation of these interesting quantitative experimental results. It is also noteworthy that these experiments [66, 67] represent one of the very early examples of computer control of experiments with automated data acquisition. [78] Without this automation it would not have been possible to obtain the results. Similarly, the use for the analysis of experimental results of

fast Fourier-transform techniques, which were still relatively new, was a novel feature of this work.

Also still unexplained is the fact that the system remains in the chaotic SV-unstable regime, instead of reducing its wavenumber so as to enter once more a regime of stable rolls which is known to exist for smaller k [62]. This latter phenomenon occurs in the one-dimensional case of a narrow rectangular cell where the SV instability leads to the expulsion of a roll pair and a consequent reduction of the wavenumber. Presumably the persistent chaos is the result of an as yet unknown wavenumber-selection process in the two-dimensional system with circular sidewalls which forces the pattern to remain in the unstable regime. Another feature of the data which was surprising at the time is that the chaos in this system was not preceded by periodic and/or quasi-periodic states which were considered typical of low-dimensional chaotic systems. [70] The absence of these states is consistent, however, with the crossing of an instability boundary which suddenly moves the system into a regime of high-dimensional chaos.

4.2 Spiral-defect chaos

In spite of its provocative early results and numerous experimental advantages [68, 69], the cryogenic work on STC had its limitations because it did not permit flow visualization. Modern experiments on RBC near ambient temperatures have used the shadowgraph method [18, 19] to visualize the temperature field associated with the convection. Recent experiments on RBC in compressed gases with Prandtl numbers σ close to one led to the discovery [24] that a chaotic state called "spiral-defect chaos" (SDC) is entered at modest ϵ when Γ is large. An example of a shadowgraph image of SDC is shown in Fig. 12a. SDC consists of many small spirals, targets, and other defects in the roll structure. The defects have a modest lifetime and drift about irregularly, and new ones are constantly created as old ones disappear. The spirals co-exist with regions of more or less straight rolls. For the ϵ value of Fig. 12a these regions have a width of only a few wavelengths; but near the onset of SDC, and particularly for very-large aspect-ratio cells [79], the straight-roll regions can become quite large. By now the SDC state has been studied in other experiments which are too numerous to list at this point. A recent review of much of this work and numerous references may be found in Ref. [22]. SDC also has been found in numerical solutions of model equations [80, 81] and of the Boussinesq equations [82]. Here I mention only one interesting aspect of this state. Figure 12b shows the azimuthal average of the structure factor $S(k)$ (square of the modulus of the Fourier transform) of SDC images. $S(k)$ can be used to compute the mean wavenumber $\bar{k}$. Results for $\bar{k}$ are shown as a function of ϵ in Fig. 12c. One can see that all the results for $\bar{k}$ lie well within the range where straight rolls are also known to be stable [65, 62]. Thus we arrive at the interesting conclusion that SDC is not caused by a bulk instability of the straight-roll patterns as apparently was the case in the smaller-aspect-ratio cryogenic experiments. Instead there is bi-stability of SDC and the usual roll state, that is over a wide parameter range straight rolls (a fixed point) as well as SDC (a chaotic attractor) are stable solutions of the

equations of motion of the system. For Prandtl numbers close to or less than one it turns out that the initial and boundary conditions of typical experiments fall within the attractor basin of SDC, and that rolls without spirals are rarely observed for ϵ greater than some onset value ϵ_s. [83]

A quantitative understanding of SDC has not been achieved so far. The problem is very difficult because the chaotic state evolves from a ground state which is already extremely complex (see, e.g., the upper left image of Fig. 10). However, some insight into the dynamics of this state has been gained. Is seems likely that mean-flow fields play a significant role. [84, 22, 85] A central feature of the dynamics seems to be the competition between two wavenumber selection processes. [81] The spiral tip selects one wavenumber, and the far field which is dominated by a number of different defect types selects another. The resulting wavenumber gradient orthogonal to the spiral arms leads to outward traveling waves surrounding the spiral tips which are equivalent to spiral rotation.

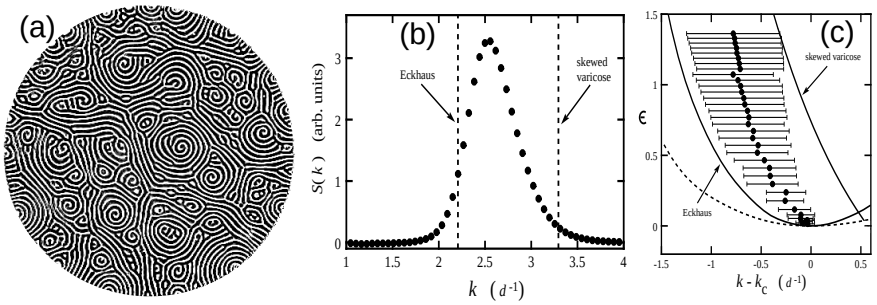

Fig. 12. Spiral-defect chaos. (a): shadowgraph image for $\Gamma = 78$, $\sigma = 0.96$, and $\epsilon = 0.72$. (b): structure factor $S(k)$ of images like that in (a), but for $\epsilon = 0.46$ (vertical dotted lines are stability boundaries of straight rolls). (c): $\bar{k}$ as a function of ϵ (solid lines are the Eckhaus and skewed-varicose instability of straight rolls; horizontal bars are the widths of $S(k)$). After Ref. [24].

5 Effect of Rotation

5.1 Domain Chaos

As mentioned in the Introduction, RBC becomes even more complex and interesting when the sample is rotated about a vertical axis. In that case the Coriolis force must be added to the equation of motion (the centrifugal force usually is neglected since to lowest order it is balanced by a pressure gradient sustained by the sidewall). The result is that, for $\Omega > \Omega_c$, the rolls that form above onset are unstable to plane-wave perturbations with a wave director which has a characteristic angle Θ_{KL} relative to the roll wave director. For $\sigma \geq 0.33$, the bifurcation is expected to be supercritical both below and above Ω_c. Thus the KL

instability offers a rare opportunity to study STC in a system where the average flow amplitude evolves continuously from zero and where weakly-nonlinear theories are expected to be applicable. After receiving only limited attention for several decades [27, 28, 29, 30, 86, 87, 88], the opportunity to study STC has led to a recent increase in activity both theoretically and experimentally [19, 31, 32, 89, 90, 91, 92, 93, 94, 95]. Indeed, as predicted theoretically,[27] the straight rolls at the onset of convection for $\Omega > \Omega_c$ are found to be unstable. In the spatially extended system this leads to the co-existance of domains of rolls of more or less uniform orientation with other domains of a different orientation. [30, 86] A typical example is shown in Fig. 13b. The replacement of a given domain of rolls proceeded primarily via domain-wall propagation. More recently the KL instability was investigated with shadowgraph flow-visualization very close to onset. It was demonstrated that the bifurcation is indeed supercritical, and that the instability leads to a continuous domain switching through a mechanism of domain-wall propagation also at small ϵ.[96, 31, 97, 32] This qualitative feature has been reproduced by Tu and Cross[91] in numerical solutions of appropriate coupled Ginzburg-Landau (GL) equations, as well as by Neufeld et al.[93] and Cross et al.[94] through numerical integration of a generalized Swift-Hohenberg (SH) equation. There is, however, also a contribution to the dynamics from nucleation of dislocation pairs *via* the KL mechanism.[98]

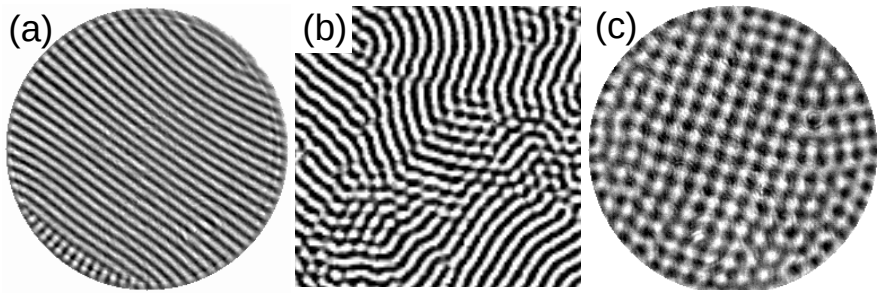

Fig. 13. Convection patterns for small ϵ. (a) is for $\Omega = 0$ and Ar gas with $\sigma = 0.69$ and $\epsilon = 0.07$ (from Ref. [35]). It shows the predicted [12] straight-roll pattern. (b) is for $\Omega = 15.4$ and CO_2 at a pressure of 32 bar with $\sigma = 1.0$ and $\epsilon = 0.05$ (from Ref. [31]). It is a typical pattern in the Küppers-Lortz-unstable range. (c) is for Argon at 40 bar with $\sigma = 0.7$, $\Omega = 145$, and $\epsilon = 0.04$ (from Ref. [33]); it shows no evidence of the Küppers-Lortz instability, and instead consists of a slowly-rotating square lattice.

Central features of the KL STC are the time and length scales of the chaotic state near onset. The GL model assumes implicitly a characteristic time dependence which varies as ϵ^{-1} and a correlation length which varies as $\epsilon^{-1/2}$. Measurements of a correlation length given by the inverse width of the square of the modulus of the Fourier transform as well as a domain-switching frequency as revealed in Fourier space yielded the data in Fig. 14.[31, 97] These results seem to be inconsistent with GL equations since they show that the time in

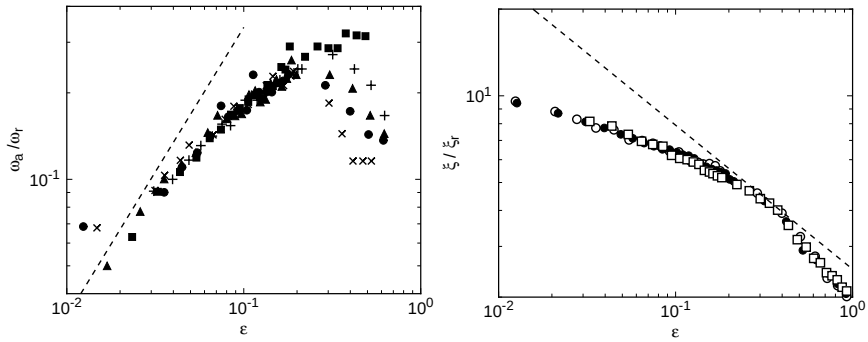

Fig. 14. The characteristic frequencies ω_a (left) and lengths ξ (right) of the KL state. The data were divided by Ω-dependent constants ω_r and ξ_r so as to collapse them onto single curves. The dashed lines are shown for reference and have the slopes 1 for ω_a and -1/2 for ξ which correspond to the theoretically expected exponents of the time and length scales near onset. The data sets cover approximately the range $14 \leq \Omega \leq 20$. See Refs. [31], [97], and [32] for details.

the experiment scales approximately as $\epsilon^{-1/2}$ and that the two-point correlation length scales approximately as $\epsilon^{-1/4}$. These results also differ from numerical results based on a generalized SH equation[94] although the range of ϵ in the numerical work is rather limited. We regard the disagreement between experiment and theory as a major problem in our understanding of STC.

5.2 Square Patterns at Modest σ

Motivated by the unexpected scaling of length and time with ϵ for the KL state at $\Omega \leq 20$, new investigations were undertaken recently in which the range of Ω was significantly extended to larger values. Contrary to theoretical predictions [29, 37, 99] based on Galerkin procedures and on the stability of appropriate coupled GL equations, it was found[33] that for $\Omega \geq 70$ the nature of the pattern near onset changed qualitatively although the bifurcation remained supercritical. Square patterns like the one shown in Fig. 13c were stable, instead of typical KL patterns like the one in Fig. 13b. The squares occurred both when Argon with $\sigma = 0.69$ was used and when the fluid was water with $\sigma \simeq 5$. They were observed as well in He-Xe gas mixtures with $\sigma \simeq 0.5$. [100] For some parameter ranges the lattice was quite disordered; but the four-fold nearest-neighbor coordination remained. The occurrence of squares in this system is completely unexpected and not predicted by theory; the KL instability should continue to be found near onset also at these higher values of Ω. Thus the experiments have uncovered a qualitative disagreement with theoretical predictions in a parameter range where one might have expected the theory to be reliable. Interestingly, very recent direct numerical simulations based on the Boussinesq equations have reproduced the square patterns near onset.[22]

A further interesting aspect of the square patterns is that the lattice rotates slowly relative to the rotating frame of the apparatus. This was found in the experiments with Argon and water [33] as well as in the simulation [22]. Measurements of the angular rotation rate ω of the lattice for the water experiment are consistent with $\omega(\epsilon)$ vanishing as ϵ goes to zero. Thus the experimental results do ot necessarily imply that the bifurcation to squares is a Hopf bifurcation. Quite possibly, as the aspect ratio of the cell diverges, the slope of $\omega(\epsilon)$ vanishes since an infinitely extended lattice can not rotate. Alternatively, of course, the lattice might become unstable as Γ becomes large. It would be interesting to study the Γ dependence of ω experimentally. To my knowledge there is as yet no theoretical explanation of this rotation.

5.3 The Range $0.16 < \sigma < 0.7$

When a RBC system is rotated about a vertical axis, the critical Rayleigh number $R_c(\Omega)$ increases. $R_c(\Omega)$ is predicted to be independent of σ, and experiment [97] and theory [1] for it are in excellent agreement as shown in fig. 15a. For $\sigma > 0.33$ the bifurcation is expected to be supercritical and to lead to KL chaos unless Ω is quite large. As discussed above in Sect. 5.2, recent experiments have shown that this is not the case; for $\Omega \geq 70$ square patterns were found which are unrelated to the typical KL domains. For large Ω and $\sigma < 0.68$, the stationary bifurcation is predicted [37] to be preceded by a supercritical Hopf bifurcation; but for $\sigma > 0.33$ experiments have not yet reached values of Ω sufficiently high to encounter time-periodic patterns.

The experimentally accessible range $0.16 \leq \sigma \leq 0.33$ is truly remarkable because of the richness of the bifurcation phenomena which occur there when the system is rotated. For instance, for $\sigma = 0.26$ there is a range from $\Omega \simeq 16$ to 190 over which the bifurcation is predicted to be subcritical. This is shown by the dashed section of the curve in Fig. 15c. The subcritical range depends on σ. In Fig. 15b it covers the area below the dashed curve. Thus, the dashed curve is a *line* of tricritical bifurcations. It has a maximum in the $\Omega - \sigma$ plane, terminating in a "tricritical endpoint". An analysis of the bifurcation phenomena which occur near it in terms of Landau equations may turn out to be interesting. One may expect path-renormalization[101] of the classical exponents in the vicinity of the maximum. We are not aware of equivalent phenomena in equilibrium phase transitions, although presumably they exist in as yet unexplored parameter ranges.

At relatively large Ω, the stationary bifurcation (regardless of whether it is super- or sub-critical) is predicted to be preceded by a supercritical Hopf bifurcation which is expected to lead to *standing* waves of convection rolls. [37] Standing waves are relatively rare; usually a Hopf bifurcation in a spatially-extended system leads to traveling waves. An example is shown by the dash-dotted line near the right edge of Fig. 3b. As can be seen there, the Hopf bifurcation terminates at small Ω at a codimension-two point on the stationary bifurcation which, depending on σ, can be super- or sub-critical. The line of codimension-two points is shown in Fig. 15b as a dash-dotted line. One sees that the tricritical line and

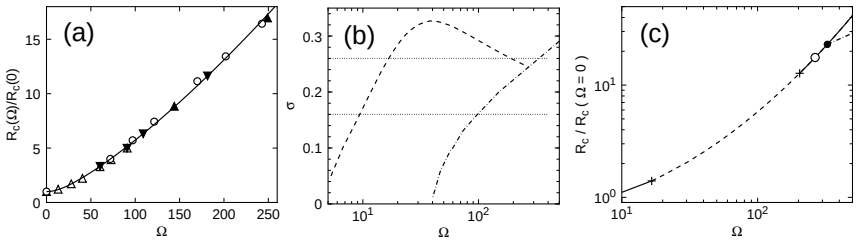

Fig. 15. The bifurcation diagram for RBC with rotation about a vertical axis. (a.) Experimental and theoretical results for $R_c(\Omega)$ obtained with water (open circles) and Ar at three different pressures (triangles) on linear scales. After Ref. [33]. (b) The theoretically predicted bifurcation diagram for RBC with rotation about a vertical axis. The dashed curve gives the tricritical line. The dash-dotted line is the codimension-two line where the Hopf bifurcation meets the stationary bifurcation (e.g. the solid circle in (c)). For $\sigma = 0.24$ the codimension-two line intersects the tricritical line, leading to the codimension-three point shown as an open circle in (c). The upper dotted line in (b) corresponds to the path represented in (c). The lower dotted line in (b) represents the lowest σ-value accessible to experiment using gas mixtures. (c) Bifurcation lines for $\sigma = 0.26$. The dashed line shows the range over which the stationary bifurcation is subcritical. The two plusses are the tricritical points. The dash-dotted line at large Ω shows the Hopf bifurcation. From Ref. [38].

the codimension-two line meet at a codimension-three point, located at $\Omega \simeq 270$ and $\sigma \simeq 0.24$. We note that this is well within the parameter range accessible to experiments. We are not aware of any experimentally-accessible examples of codimension-three points. This particular case should be accessible to analysis by weakly-nonlinear theories, and a theoretical description in terms of GL equations would be extremely interesting and could be compared with experimental measurements.

The σ-range of interest is readily accessible to us by using mixtures of a heavy and a light gas.[36] Values of σ *vs.* the mole fraction x of the heavy component for a typical pressure of 22 bar and at 25 °C are shown in Fig. 4. An important question in this relation is whether the mixtures will behave in the same way as pure fluids with the same σ. We believe that to a good approximation this is the case because the Lewis numbers are of order one. This means that heat diffusion and mass diffusion occur on similar time scales. In that case, the concentration gradient will simply contribute to the buoyancy force in synchrony with the thermally-induced density gradient, and thus the critical Rayleigh number will be reduced. Scaling bifurcation lines by $R_c(\Psi)$ (Ψ is the separation ratio of the mixture) will mostly account for the mixture effect. To a limited extent we showed already that this is the case.[35, 36] In more recent work we have begun to show that the bifurcation line $R_c(\Omega)/R_c(0)$ is independent of Ψ. Nonetheless we recognize that a theoretical investigation of this issue will be very important.

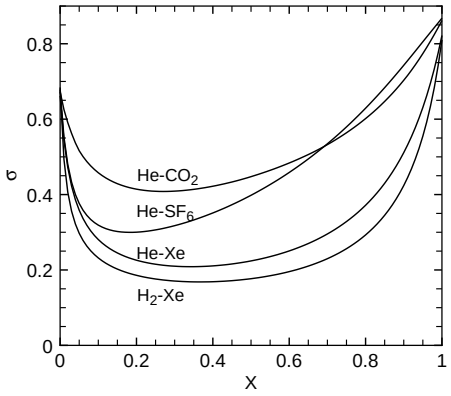

Fig. 16. The Prandtl number σ as a function of the mole fraction x of the heavy component for three gas mixtures at a pressure of 22 bar and at 25 °C. From Ref. [36].

Assuming that the mixtures behave approximately like pure fluids, we see that the codimension-three point can be reached using either H_2-Xe or He-Xe mixtures. The tricritical point can be reached also using He-SF_6.

6 Conclusion

In these few pages it has been possible to touch only on a few of the interesting aspects of RBC. Some others are discussed in this volume in the chapter by P. Manneville; but even collectively these two contributions do not constitute a thorough review of the field. Nonetheless it is clear that a century of research since the original work of Henri Bénard on this conceptually simple system has strongly advanced our understanding of spatially extended nonlinear dissipative systems. However, much remains to be done. For example, the study of external noise on the system is in its infancy. We believe that the bifurcation to RBC becomes subcritical in the presence of noise, but the influence of noise on the "ordered" state (i.e. the convection rolls) has been examined only qualitatively. It also is apparent that there is a number of unsolved problems. Although we have learned a lot from studies of SDC and domain chaos, the general nature of STC is not understood at a quantitative level. Important issues are whether a description in terms of general principles, perhaps analogous to those of equilibrium statistical mechanics, is on the horizon. [102] We also saw that there are several specific issues on which theory and experiment conflict. These include the characteristic length and time scales of domain chaos and the occurrence at onset of square patterns in the presence of rotation. It will be interesting for future generations of physicists to see what the next century will bring.

References

1. For interesting historical notes on this topis, see S. Chandrasekhar, *Hydrodynamic and Hydromagnetic Stability*, (Oxford University Press, London, 1961).
2. H. Bénard, *Rev. Gen. Sci. Pure Appl.* **11**, 1261(1900); 1309 (1900); *Ann. Chim. Phys.* **23**, 62 (1901).
3. For examples, see the article by P. Manneville in this volume, and Ref. [1].
4. Lord Rayleigh, Phil. Mag. **32**, 529 (1916).
5. H. Jeffreys, Phil. Mag. **2**, 833 (1926); Proc. Roy. Soc. (London) A **118**, 195 (1928).
6. J. Oh and G. Ahlers, unpublished.
7. K.M.S. Bajaj, N. Mukolobwiez, N. Currier, and G. Ahlers, *Phys. Rev. Lett.* **83**, 5282 (1999).
8. M.A. Dominguez-Lerma, G. Ahlers, and D.S. Cannell, *Phys. Rev. E.* **52**, 6159 (1995).
9. W. V. R. Malkus and G. Veronis, *J. Fluid Mech.* **38**, 227 (1958).
10. J. Boussinesq, *Théorie Analytique de la Chaleur*, vol.2. (Gauthier-Villars, Paris, 1903).
11. A. Oberbeck, *Ann. Phys. Chem.* **7**, 271 (1879).
12. A. Schlüter, D. Lortz, and F. Busse, *J. Fluid Mech.* **23**, 129(1965).
13. P. L. Silveston, Forsch. Ing. Wes. **24**, 29 (1958); 59 (1958).
14. G. Ahlers, unpublished.
15. J.B. Swift and P.C. Hohenberg, *Phys. Rev. A* **15**, 319 (1977).
16. J. Oh and G. Ahlers, unpublished.
17. R. J. Schmidt and S. W. Milverton, *Proc. Roy. Soc. (London) A* **152**, 586 (1935).
18. S. Rasenat, H. Hartung, B.L. Winkler, and I. Rehberg, *Experiments in Fluids* **7**, 412 (1989).
19. J. R. de Bruyn, E. Bodenschatz, S. W. Morris, S. Trainoff, Y. Hu, D. S. Cannell, and G. Ahlers, Rev. Sci. Instrum. **67**, 2043 (1996).
20. S.P. Trainoff and D.S. Cannell. Phys. Fluids **14**, 1340 (2002).
21. For a recent review, see for instance, M. C. Cross and P.C. Hohenberg, *Rev. Mod. Phys.* **65**, 851 (1993).
22. For a recent review of pattern formation in gas convection, see E. Bodenschatz, W. Pesch, and G. Ahlers, *Annu. Rev. Fluid Mech.* **32**, 709 (2000).
23. V. Croquette, Contemp. Phys. **30**, 113 (1989); **30**, 153 (1989).
24. S. W. Morris, E. Bodenschatz, D. S. Cannell, and G. Ahlers, Phys. Rev. Lett. **71**, 2026 (1993).
25. R. Krishnamurty, J. Fluid Mech. **42**, 295 (1970); 309 (1970).
26. R. Krishnamurty, J. Fluid Mech. **60**, 285 (1973).
27. G. Küppers and D. Lortz, J. Fluid Mech. **35**, 609 (1969).
28. G. Küppers, Phys. Lett. **32A**, 7 (1970).
29. R.M. Clever and F.H. Busse, J. Fluid Mech. **94**, 609 (1979).
30. F.H. Busse and K.E. Heikes, Science **208**, 173 (1980); K.E. Heikes and F.H. Busse, Ann. N.Y. Acad. Sci. **357**, 28 (1980).
31. Y. Hu, R.E. Ecke, and G. Ahlers, Phys. Rev. Lett. **74**, 5040 (1995); and Phys. Rev. E **55**, 6928 (1997).
32. Y. Hu, W. Pesch, G. Ahlers, and R.E. Ecke, Phys. Rev. **58**, 5821 (1998).
33. K. M. S. Bajaj, J. Liu, B. Naberhuis, and G. Ahlers, Phys. Rev. Lett. **00**, 00 (1998).
34. One exception is liquid helium. As the superfluid-transition temperature 2.176 K is approached from above, σ vanishes. However, experiments are difficult because σ varies from a value of order one to zero over a narrow temperature range of a few

mK, and because of the problem of flow visualization, which has only recently been achieved under the required cryogenic conditions (P. Lucas, A. Woodcraft, R. Matley, and W. Wong, International Workshop on Ultra-High Reynolds-Number Flows, Brookhaven National Laboratory, June 18 to 20, 1996). Other exceptions are liquid metals which have $\sigma = \mathcal{O}(10^{-2})$ because of the large electronic contribution to the conductivity. However, it is not possible to explore the range $10^{-2} \leq \sigma \leq 0.7$ with them. Since liquid metals are not transparent to visible light, flow visualization is also a problem.
35. J. Liu and G. Ahlers, Phys. Rev. Lett. **77**, 3126 (1996).
36. J. Liu and G. Ahlers, Phys. Rev. E **55**, 6950 (1997).
37. T. Clune and E. Knobloch, Phys. Rev. E **47**, 2536 (1993).
38. K.M.S. Bajaj, G. Ahlers, and W. Pesch, Phys. Rev. E **65**, 056309 (2002).
39. F.H. Busse and R.M. Clever, *J. Eng. Math.* **26**, 1 (1992).
40. R.E. Kelly, *Adv. in Appl. Mech.* **31**, 35 (1994).
41. L.D. Landau and E.M. Lifshitz, *Fluid Mechanics* (Pergamon, London, 1959).
42. I. Rehberg, S. Rasenat, M. de la Torre-Juarez, W. Schöpf, F. Hörner, G. Ahlers, and H.R. Brand, *Phys. Rev. Lett.* **67**, 596 (1991).
43. E. Bodenschatz, S. Morris, J. de Bruyn, D.S. Cannell, and G. Ahlers, in *Proceedings of the KIT International Workshop on the Physics of Pattern Formation in Complex Dissipative Systems*, ed. S. Kai (World Scientific, Singapore, 1992), p. 227.
44. M. Wu, G. Ahlers, and D.S. Cannell, *Phys. Rev. Lett.* **75**, 1743 (1995).
45. Recent measurements by W. Schöpf and I. Rehberg [*J. Fluid Mech.* **271**, 235 (1994)] using binary mixtures and by G. Quentin and I. Rehberg [*Phys. Rev. Lett.* **74**, 1578 (1995)] involved pseudo-one-dimensional sample geometries for which theoretical predictions are more difficult to obtain due to the influence of the sidewalls. In this review we consider only results obtained for systems of large extent in two dimensions.
46. H. van Beijeren and E.G.D. Cohen, *J. Stat. Phys.* **53**, 77 (1988).
47. P. C. Hohenberg, and J. Swift, *Phys. Rev. A* **46**, 4773 (1992).
48. M. A. Scherer, G. Ahlers, F. Hörner, and I. Rehberg, *Phys. Rev. Lett.* **85**, 3754 (2000).
49. M.A. Scherer and G. Ahlers, *Phys. Rev. E* **65**, 051101 (2002).
50. S. A. Brazovskii, *Sov. Phys. JETP* **41**, 85 (1975).
51. F. S. Bates, J. H. Rosedale, G. H. Fredrickson, and C. J. Glinka, *Phys. Rev. Lett.* **61**, 2229 (1988).
52. This feature was noted also by M. Assenheimer and V. Steinberg, *Europhysics News* **27**, 143 (1996).
53. These results differ from measurements by Roy and Steinberg,[54] who found hexagons just above onset for seemingly similar experimental parameters.
54. A. Roy and V. Steinberg, *Phys. Rev. Lett.* **88**, 244503-1 (2002).
55. D. A. Egolf, I. V. Melnikov, and E. Bodenschatz, Phys. Rev. Lett. **80**, 3228 (1998).
56. J. Toner and D.R. Nelson, Phys. Rev. B **23**, 316 (1981).
57. F. Busse, J. Fluid Mech. **30**, 625 (1967).
58. E. Bodenschatz, J. R. de Bruyn, G. Ahlers, and D. S. Cannell, Phys. Rev. Lett. **67**, 3078 (1991).
59. On the basis of these results it seems likely that the hexagons reported by A. Roy and V. Steinberg, Phys. Rev. Lett. **88**, 244503 (2002) are caused by non-Boussinesq effects due to a non-critical density in their experiment rather than by compressibility effects as suggested by these authors.
60. J. Liu, K.M.S. Bajaj, and G. Ahlers, unpublished.

61. Y. Hu, R. Ecke, and G. Ahlers, Phys. Rev. E **48**, 4399 (1993); Phys. Rev. Lett. **72**, 2191 (1994), Phys. Rev. Lett. **74**, 391 (1995); Phys. Rev. E **51**, 3263 (1995).
62. F.H. Busse and R.M. Clever, J, Fluid Mech. **91**, 319 (1979).
63. G. Ahlers and R.P. Behringer, Phsy. Rev. Lett. **40**, 712 (1978).
64. G. Ahlers and R.W. Walden, Phys. Rev. Lett. **44**, 445 (1980).
65. R. M. Clever and F. H. Busse, J. Fluid Mech. **65**, 625 (1974).
66. G. Ahlers, Bull. Am. Phys. Soc. **17**, 59 (1972).
67. G. Ahlers and J.E. Graebner, Bull. Am. Phys. Soc. **17**, 61 (1972).
68. G. Ahlers, in *Fluctuations, Instabilities, and Phase Transitions*, edited by T. Riste (Plenum, NY, 1974), p. 181.
69. G. Ahlers, Phys. Rev, Lett. **33**, 1185 (1974).
70. J. Gollub and H.L. Swinney, Phys. Rev. Lett. **35**, 927 (1975).
71. A. Libchaber and J. Maurer, J. Phys. Colloq. C3 **41**, C3-51 (1978).
72. M. Feigenbaum, J. Stat. Phys. **19**, 25 (1978).
73. An overview of dynamical systems and temporal chaos can be found, for instance, in *Order within Chaos*, P. Bergé, Y. Pomeau, and C. Vidal (Wiley, NY, 1986).
74. See, for instance, P.C. Hohenberg and B.I. Shraiman, Physica D **37**, 109 (1989); and J. P. Gollub, Nature **367**, 318 (1994).
75. H.S. Greenside, G. Ahlers, P.C. Hohenberg, and R.W. Walden, Physica **5D**, 322 (1982).
76. U. Frisch and R. Morf, Phys. Rev. A **23**, 2673 (1981).
77. For a recent discussion of the extensive nature of STC, see D.A. Egolf, I.V. Melnikov, W. Pesch, and R.E. Ecke, Nature **404**, 733 (2000).
78. B.D. Wonsiewicz, A.R. Storm, and J.D. Sieber. Bell Syst. Tech. J. **57**, 2209 (1978).
79. J. Liu and G. Ahlers, unpublished.
80. H.-W. Xi, J.D. Gunton, and J. Vinals, Phys. Rev. Lett. **71**, 2030 (1993).
81. M.C. Cross and Y. Tu, Phys. Rev. Lett. **75**, 834 (1995).
82. W. Decker, W. Pesch, and A. Weber, Phys. Rev. Lett. **73**, 648 (1994).
83. See, however, R.V. Cakmur, D.A. Egolf, B.B. Plapp, and E. Bodenschatz (to be published) where the bi-stability of straight rolls and SDC was demonstrated experimentally.
84. I.V. Melnikov and W. Pesch, unpublished.
85. K.-H. Chiam, M.R, Paul, and M.C. Cross, Phys. Rev. E **67**, 056206 (2003).
86. K. E. Heikes and F. H. Busse, Ann. N.Y. Acad. Sci. **357**, 28 (1980).
87. K. Buhler and H. Oertel, J. Fluid Mech. **114**, 261 (1982).
88. J. J. Niemela and R. J. Donnelly, Phys. Rev. Lett. **57**, 2524 (1986).
89. F. Zhong, R. Ecke, and V. Steinberg, Physica D **51**, 596 (1991).
90. F. Zhong and R. Ecke, Chaos **2**, 163 (1992).
91. Y. Tu and M. Cross, Phys. Rev. Lett. **69**, 2515 (1992).
92. M. Fantz, R. Friedrich, M. Bestehorn, and H. Haken, Physica D **61**, 147 (1992).
93. M. Neufeld, R. Friedrich, and H. Haken, Z. Phys. B. **92**, 243 (1993).
94. M. Cross, D. Meiron, and Y. Tu, Chaos **4**, 607 (1994).
95. Y. Ponty, T. Passot, and P. Sulem, Phys. Rev. Lett. **00**, 00 (1997).
96. E. Bodenschatz, D. S. Cannell, J. R. de Bruyn, R. Ecke, Y. Hu, K. Lerman, and G. Ahlers, Physica D **61**, 77 (1992).
97. Y. Hu, R. E. Ecke, and G. Ahlers, Phys. Rev. E **55**, 6928 (1997).
98. N. Becker and G. Ahlers, unpublished.
99. W. Pesch, private communication.
100. K.M.S. Bajaj and G. Ahlers, unpublished.
101. M. E. Fisher, Phys. Rev. **176**, 257 (1968).
102. See, for instance, D.A. Egolf, Science **296**, 1813 (2002).